Technical Report No. 32-149

# The Aperture Efficiency of Large Paraboloidal Antennas As a Function of Their Feed-System Radiation Characteristics

P. D. Potter

jpl
JET PROPULSION LABORATORY
CALIFORNIA INSTITUTE OF TECHNOLOGY
PASADENA, CALIFORNIA

September 25, 1961

9163 - 85404

NATIONAL AERONAUTICS AND SPACE ADMINISTRATION
(NASA CONTRACT ~~NO.~~ NASw-6)

; JPL-TR-32-149)
Technical Report No. 32-149

all caps

# The Aperture Efficiency of Large Paraboloidal Antennas As a Function of Their Feed-System Radiation Characteristics

P. D. Potter

[7]

R. Stevens

R. Stevens, Chief
*Communications Elements Research*

4742003

JET PROPULSION LABORATORY
CALIFORNIA INSTITUTE OF TECHNOLOGY
PASADENA, CALIFORNIA

September 25, 1961 24 p 10 refs

## CONTENTS



## FIGURES

## ABSTRACT

A simple graphical technique has been developed for the determination of paraboloidal antenna efficiency as a function of the feed-system radiation characteristics. The technique, based on graphical integration of the paraboloid surface current density, is applied in detail to the Cassegrainian feed system—a system which is used with low-noise antennas to maximize the ratio of antenna efficiency to system noise temperature. The discussion includes an analysis of errors involved in the calculation of antenna efficiency: polarization loss, aperture phase errors, azimuthal sampling errors, and aperture blockage.


## I. INTRODUCTION

With the advent of interplanetary space communications systems, and their critical dependence on the performance of very large ground-based paraboloidal antennas, it has become pertinent to develop new analytical techniques for relating feed radiation patterns to secondary pattern gain. A number of workers have developed analytical techniques for approximating this relationship for a few simple types of feed radiation patterns (Ref. 1, 2). Unfortunately, the functions assumed for the feed radiation patterns seldom bear a close relationship to those obtained in practice. This may be especially true in low-noise antennas in which shaped-beam or Cassegrainian feed systems are used to maximize the ratio of antenna efficiency to system noise temperature.

It appears that an accurate but simple graphical technique must be developed to relate experimental feed radiation characteristics to the over-all antenna gain. In Sec. II such a technique is developed, based on graphical integration of the paraboloid surface current density. In Sec. III the method is applied to the special but important case of a Cassegrainian system. In Sec. IV a brief analysis of the approximations and errors is made.

## II. THE GRAPHICAL INTEGRATION TECHNIQUE

The paraboloidal reflector antenna geometry is depicted in Fig. 1. The reflector surface itself is characterized by the spherical coordinates $\rho$, $\psi$, and $\xi$, with the origin at the focal point $F$. The surface is also characterized by the rectangular coordinate system $X$, $Y$, and $Z$, with the origin at the vertex of the paraboloid. The secondary radiation is described in the spherical coordinate system $R$, $\theta$, and $\phi$.

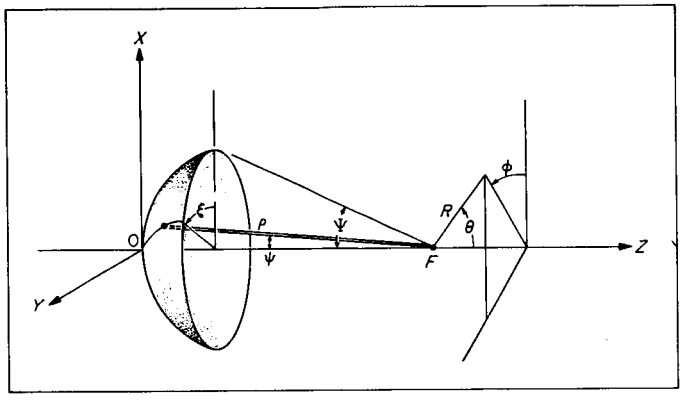


**Figure 1. Paraboloidal antenna geometry**

The expression for antenna efficiency, $\eta$, derived in Appendix A, is

$$\eta = \cot^2\left(\frac{\Psi}{2}\right) G_{0f} \left| \frac{1}{N} \sum_{n=1}^{n=N} \int_0^{\Psi} E_{fn}(\psi, \xi_n) \tan\left(\frac{\psi}{2}\right) d\Psi \right|^2 \tag{1}$$

In this expression, $G_{0f}$ is the feed-system maximum gain relative to the isotropic level, and $E_{fn}$ is a particular feed radiation pattern obtained in a plane defined by $\xi$ = constant. The assumptions and approximations implicit in Eq. (1) are described in Sec. IV. In general, the accuracy of Eq. (1) appears to be comparable to experimental measurement techniques, at least for the case of very large antennas.

As a practical matter, it is desirable to have a simple graphical technique for computing $\eta$ as a function of the parameters $\Psi$, $G_{0f}$, and $E_{fn}$. Three different situations may exist. In the first, all three parameters are unknown and varied to optimize Eq. (1), possibly subject to some constraint such as low excess-noise temperature. This problem is extremely complex and beyond the scope of this report. The second situation involves the choice of $E_{fn}$ (and hence of $G_{0f}$) to optimize Eq. (1) when the aperture angle $\Psi$ is fixed. This case will be touched upon in connection with the Cassegrainian feed system, but will not be considered in great detail. The third situation, in which $\Psi$ is fixed and $E_{fn}$ and $G_{0f}$ have been experimentally determined, is the principal subject under consideration in this report. In this case it is possible to use a rather simple graphical integration technique to perform the integration indicated in Eq. (1).

Consider a rectangular plot as shown in Fig. 2. The integrand of Eq. (1) is plotted linearly as the ordinate $h$ and the aperture angle is plotted linearly as the abscissa $w$. The incremental area of a small vertical strip will be given by

$$\Delta A = h \Delta w \tag{2}$$

A new abscissa coordinate, $w'(\psi)$, is now defined such that

$$h \tan\left(\frac{w}{2}\right) \Delta w = h \Delta w'(\psi) \tag{3}$$

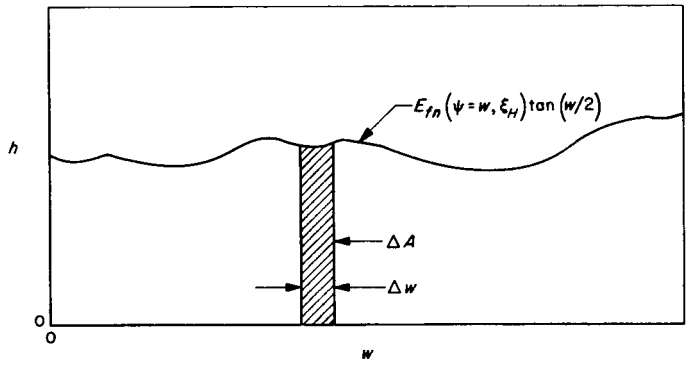


**Figure 2. Aperture integration geometry**

Passing into the limit of zero increment size and integrating both sides of Eq. (3), one obtains

$$\int_0^{w=\Psi} \tan\left(\frac{w}{2}\right) dw = \int_0^{w'(\psi)} dw'(\psi) \tag{4}$$

or

$$w'(\psi) = 2 \ln \left| \sec \frac{\Psi}{2} \right| \tag{5}$$

With the aid of Eq. (5), a weighted graph paper may be constructed such that if $E_{fn}$ is plotted, the area under the curve will be proportional to the corresponding integral in Eq. (1). A sample of this type of paper is shown in Fig. 3. The integration may be conveniently performed to high accuracy with an ordinary desk planimeter.

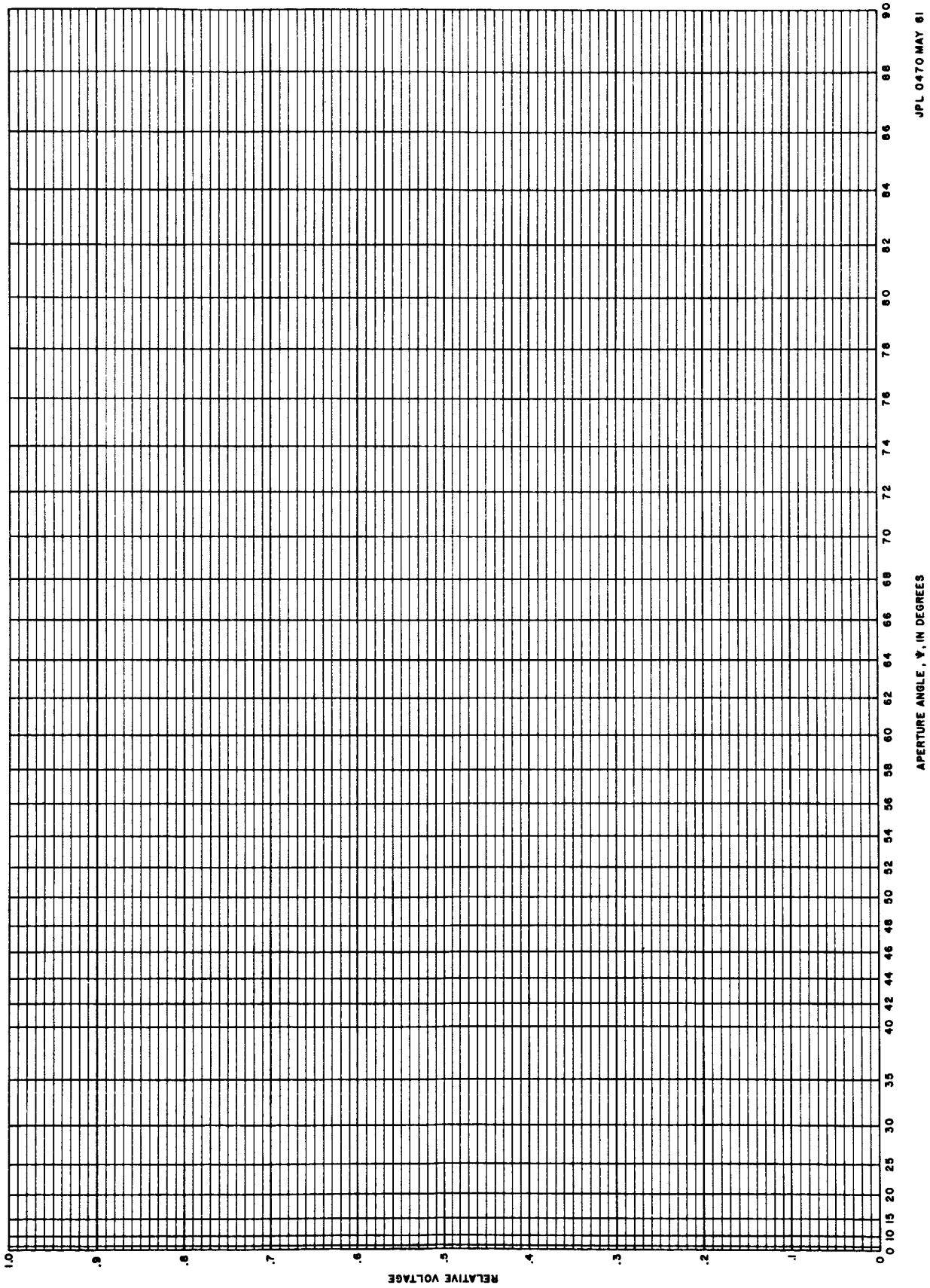


**Figure 3. Sample of weighted aperture integration paper**

In order to establish the numerical value of the integral, it is necessary to know the value of the integral for $E_{fn} = 1$ or, in other words, the value of

$$I_{n0}(\Psi) = \int_0^{\Psi} \tan \frac{\Psi}{2} d\psi \qquad (6)$$

A graph of $I_{n0}(\Psi)$ from 0 to 90 deg is shown in Fig. 4.

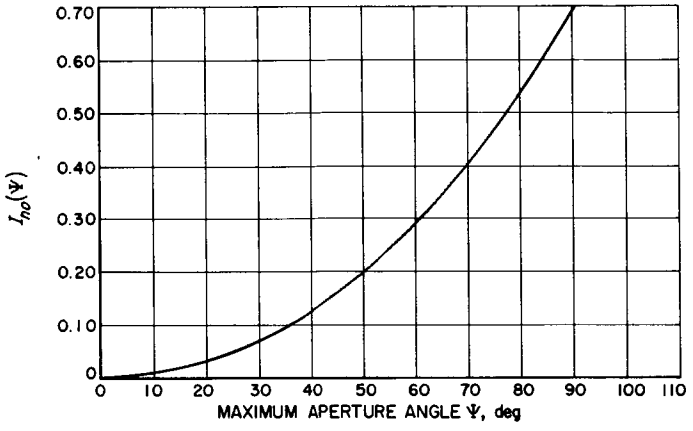


**Figure 4. Plot of the function $I_{n0}(\Psi)$ vs $\Psi$**

The calculation, therefore, of the efficiency $\eta$ involves the performance of the following steps:

1. Determination by measurement or otherwise of the absolute feed gain $G_{0f}$.
2. Determination by measurement or otherwise of the feed radiation patterns $E_{fn}(\psi, \xi)$.
3. Graphical integration of the feed patterns and normalization with the aid of Eq. (6).
4. Calculation of the efficiency by Eq. (1).

As a less accurate alternative to measurement of $G_{0f}$, the power patterns $E^2_{fn}(\psi)$ may be integrated to obtain $G_0(f)$ (assuming negligible losses). Some error will be introduced because of the cross-polarization component. This point is discussed in more detail in Sec. IV. The feed gain will be given by

$$G_{0f} = \frac{\sum_{n=1}^{n=N} \int_0^{180°} E^2_{fn}(\psi, \xi_n) \sin \psi \, d\psi}{N \int_0^{180°} \sin \psi \, d\psi} \qquad (7)$$

In a manner analogous to that of Eq. (2) through (6), it is possible to construct a weighted graph paper to provide a means of directly evaluating Eq. (7) with a planimeter. A sample of this paper is shown in Fig. 5. The vertical scale is also weighted so that the relative voltage pattern $E_{fn}$ may be plotted directly.

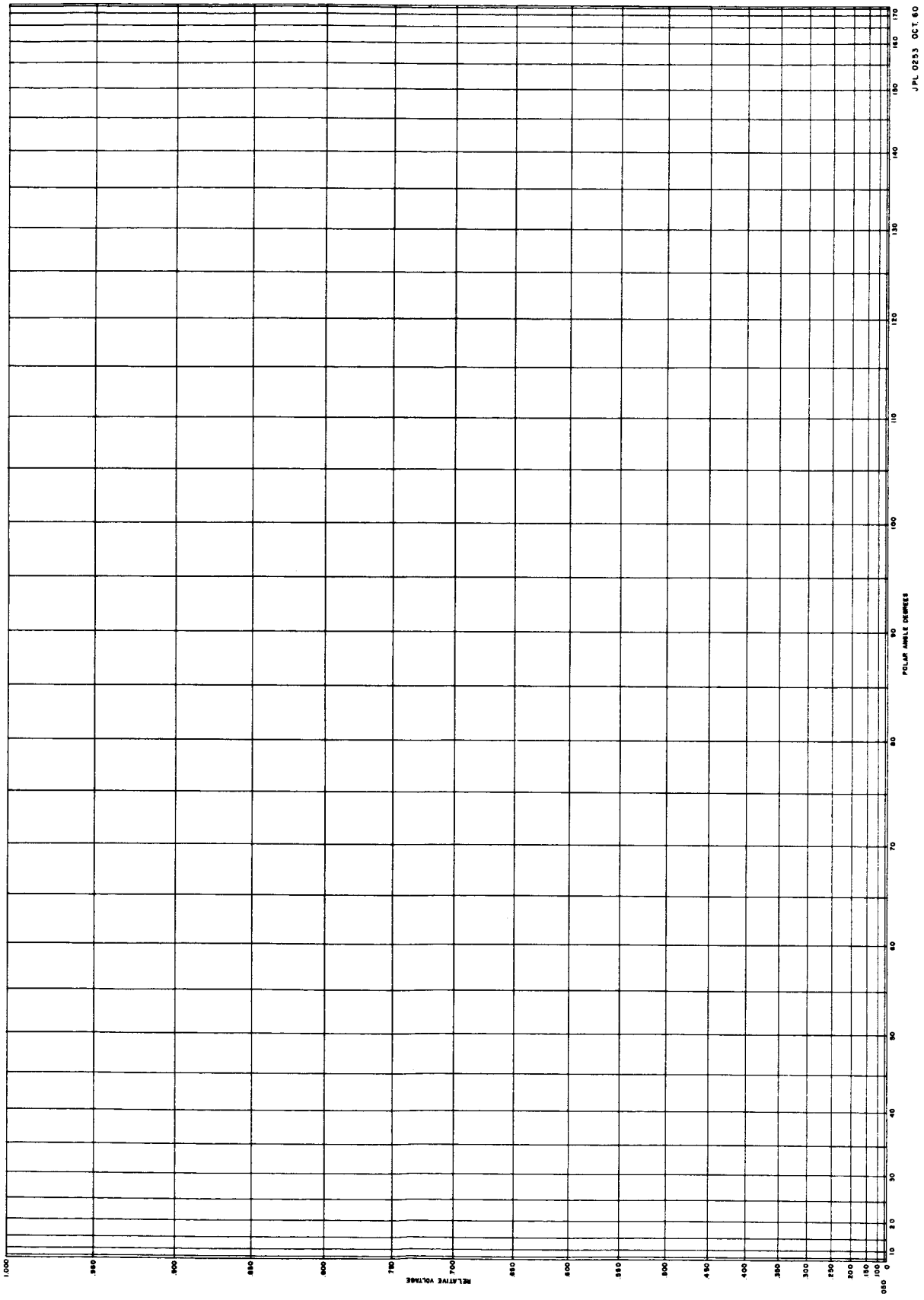


Figure 5. Sample of weighted directivity integration paper

# III. APERTURE INTEGRATION FOR A CASSEGRAINIAN SYSTEM

The increasing popularity of the Cassegrainian optics system at radio frequencies has lent new importance to its evaluation. The unusual ability of this type of feed system to produce high efficiency and low back-radiation was first recognized by Foldes (Ref. 3). Further extension of this early work has led to low-noise antenna system applications (Ref. 4). A recent and comprehensive paper by Hannon (Ref. 5) describes the general properties of the system, as well as some experimental results.

The efficiency of a Cassegrainian system as a function of its size, geometrical parameters, and feedhorn design is of key importance. A detailed analysis of the problem from the physical optics standpoint is desirable but difficult, although some work has been done toward this end (Ref. 4, 6). For the important case in which the subreflector is many wavelengths in size, geometrical optics yields sufficiently accurate answers for prototype feedhorn and subreflector design. With the prototype feedhorn and subreflector, the necessary data for Eq. (1) can be determined experimentally. Thus, the over-all efficiency may be relatively accurately predicted prior to final measurement of the antenna system.

The geometry of the Cassegrainian system is shown in Fig. 6. A feedhorn whose phase center is at the point $F'$ illuminates the subreflector, which, in turn, illuminates the paraboloid. The locus of points with a constant difference of the distance from $F$ and $F'$ is a hyperboloid of revolution. Since $F$ is the focal point of the paraboloid, this geometry will result in equal ray length from the point $F'$ to any point in the aperture plane. Also, all rays will emerge parallel to the axis of the system. Thus, the system transforms a spherical wavefront with center at $F'$ into a new spherical wave with center at $F$ (within the limitations of geometrical optics that all radii of curvature and regions of large amplitude change are very large compared to a wavelength). As will be seen later, the feedhorn amplitude illumination function is also expanded and reshaped. It is this latter property that makes practical the achievement of unusually high efficiency.

The geometry of the hyperboloid in the Cartesian coordinate system shown in Fig. 6 is given by

$$\frac{Z_H^2}{a^2} - \frac{X_H^2 + Y_H^2}{c^2 - a^2} = 1 \tag{8}$$

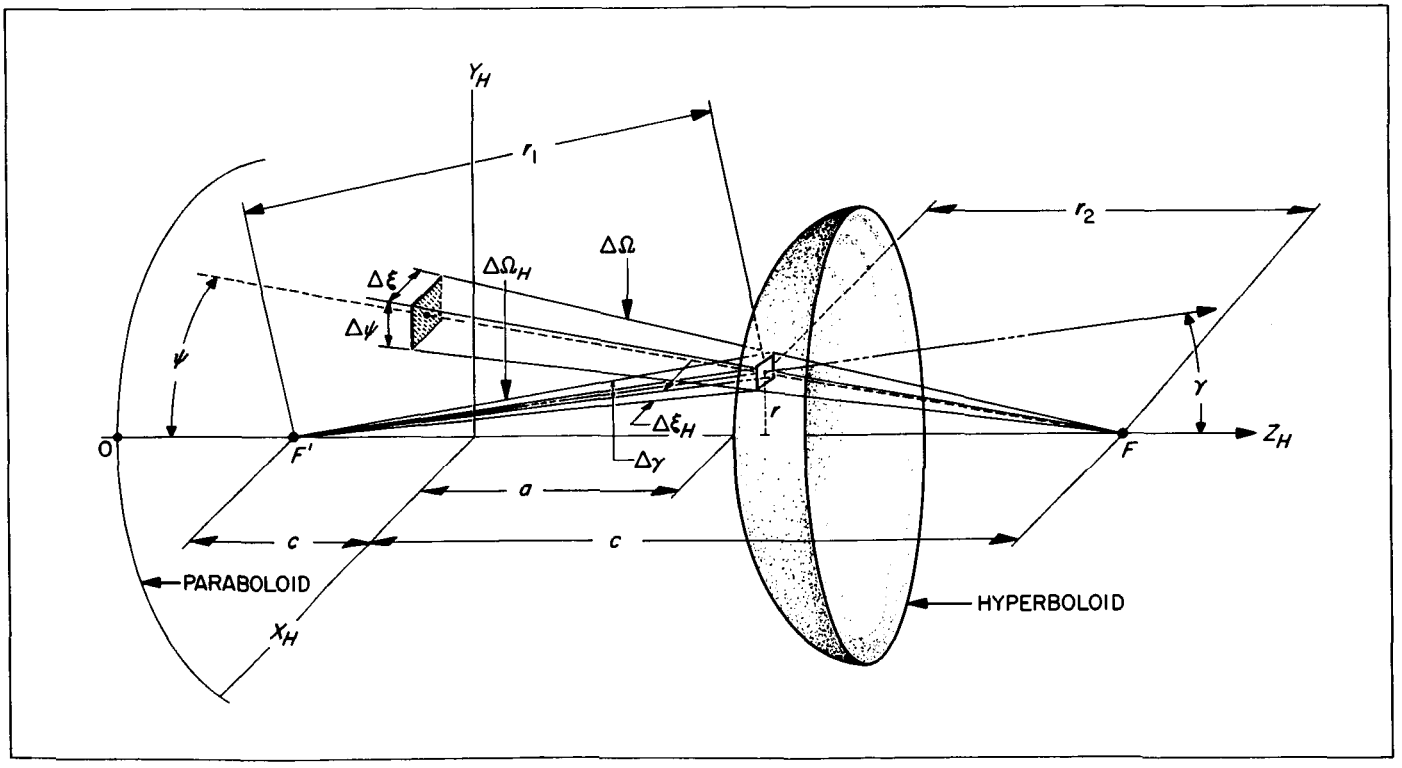


**Figure 6. Cassegrainian optics geometry**

or

$$\frac{Z^2}{a^2} - \frac{r^2}{c^2 - a^2} = 1 \tag{9}$$

The angles $\gamma$ and $\psi$ are related by

$$\tan\left(\frac{\psi}{2}\right) = M \tan\left(\frac{\gamma}{2}\right) \tag{10}$$

where $M$ is a constant called the magnification and is usually large compared to unity.

The transformation of the feedhorn gain function $G_H(\gamma, \xi_H)$ into the subreflector gain function $G_f(\psi,\xi)$ will now be investigated on a geometrical optics basis. In this approximation an incremental ray bundle of solid angle $\Delta\Omega_H$ is defined, which is transformed by the hyperboloid into a new incremental ray bundle $\Delta\Omega$. By definition no energy crosses the walls of these two bundles.

The feed power radiated per unit solid angle is given by

$$P_H(\gamma, \xi_H) = \frac{G_H(\gamma, \xi_H)}{4\pi} P_T \tag{11}$$

and the subreflector radiated power per unit solid angle is given by

$$P(\psi, \xi) = \frac{G_f'(\psi, \xi)}{4\pi} P_{TF} \tag{12}$$

Since no energy crosses the side boundaries of the ray bundles, the following relationship exists:

$$P_H(\gamma, \xi_H)\,\Delta\Omega_H = P(\psi, \xi)\,\Delta\Omega \tag{13}$$

or

$$G_f'(\psi, \xi) = \frac{\Delta\Omega_H}{\Delta\Omega} \frac{P_T}{P_{TF}} G_H(\gamma, \xi_H) \tag{14}$$

where

$$\frac{P_T}{P_{TF}} = \frac{\displaystyle\int_0^{2\pi}\int_0^{\pi} G_H(\gamma, \xi_H) \sin\gamma\, d\gamma\, d\xi_H}{\displaystyle\int_0^{2\pi}\int_0^{\gamma_0} G_H(\gamma, \xi_H) \sin\gamma\, d\gamma\, d\xi_H} \tag{15}$$

It is now necessary to evaluate the quantity $\Delta\Omega_H/\Delta\Omega$. The solid angle $\Delta\Omega_H$ is bounded by the four rays which are $\pm\Delta\gamma/2$ and $\pm\Delta\xi_H/2$ from the central ray. Thus

$$\Delta\Omega_H \approx \Delta\gamma\,\Delta\xi_H \tag{16}$$

Similarly,

$$\Delta\Omega \approx \Delta\psi\,\Delta\xi \tag{17}$$

Now from Fig. 6 it can be seen that

$$\Delta\xi_H \approx \frac{\Delta l_1}{r_1} \tag{18}$$

$$\Delta\xi = \frac{\Delta l_1}{r_2} \tag{19}$$

where $\Delta l_1$ is an incremental distance on the hyperboloid. Since $\Delta l_r$ bisects the angle between $F'P$ and $FP$, then

$$\begin{aligned} \Delta\gamma &= \frac{\Delta l_r}{r_1} \cdot \mathbf{n} \cdot \mathbf{r}_2 \\ \Delta\psi &= \frac{\Delta l_r}{r_2} \cdot \mathbf{n} \cdot \mathbf{r}_2 \end{aligned} \tag{20}$$

Combining Eq. (16) through (20) yields

$$\frac{\Delta\Omega_H}{\Delta\Omega} = \left(\frac{r_2}{r_1}\right)^2 \tag{21}$$

From Fig. 6 it can be noted that

$$r_1 = \frac{r}{\sin\gamma} \tag{22}$$

$$r_2 = \frac{r}{\sin\psi} \tag{23}$$

Combining Eq. (14), (21), (22), and (23),

$$G_f'(\psi, \xi) = \frac{P_T}{P_{TF}} \left(\frac{\sin\gamma}{\sin\psi}\right)^2 G_H(\gamma, \xi_H) \tag{24}$$

where $\psi$ and $\gamma$ are related by Eq. (10) and $\xi_H = \xi$.

It was assumed, however, in the derivation of Eq. (1) (see Eq. A-6 and A-7 in Appendix A) that the total antenna power was delivered into the radiation defined by Eq. (24). To convert Eq. (24) into an "equivalent" gain function $G_f$ that may be used in Eq. (1), it is necessary to multiply Eq. (24) by $P_{TF}/P_T$:

$$G_f(\psi, \xi) = \left(\frac{\sin\gamma}{\sin\psi}\right)^2 G_H(\gamma, \xi_H) \tag{25}$$

where $\psi$ and $\gamma$ are related by Eq. (10) and $\xi_H = \xi$. If, as is usually the case, $\gamma$ is less than 15 deg, then with only 2% maximum error,

$$\sin\gamma \approx 2\tan\frac{\gamma}{2} \tag{26}$$

Combining Eq. (10), (25), and (26) gives

$$G_f(\psi, \xi) \approx \frac{1}{M^2}\left(\frac{2\tan\frac{\psi}{2}}{\sin\psi}\right)^2 G_H(\gamma, \xi_H) = \frac{1}{M^2}\sec^4\left(\frac{\psi}{2}\right) G_H(\gamma, \xi_H) \tag{27}$$

A plot of the function $\sec^4(\psi/2)$ is shown in Fig. 7. The significance of Fig. 7 is that the Cassegrainian geometry tends to weight the outer portions of the aperture more heavily than the inner portions. This effect is beneficial in obtaining high efficiency, since the paraboloid spillover may be independently adjusted by means

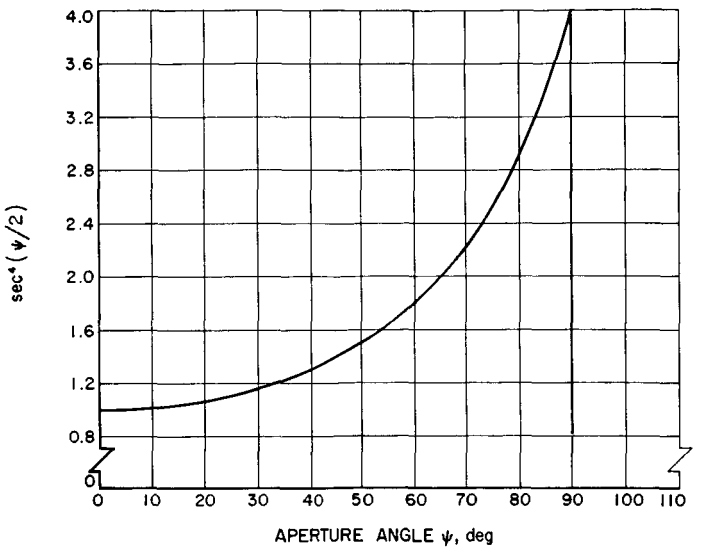


**Figure 7. Cassegrainian weighting function $\sec^4(\psi/2)$**

of the hyperboloid aperture angle. A further beneficial factor can be observed in Fig. 8, which is a plot of Eq. (10). It can be seen that the relatively flat central portion of the feedhorn pattern tends to be expanded onto a disproportionately large portion of the paraboloid aperture.

It is interesting to consider the feedhorn radiation pattern which would yield uniform aperture illumination and hence maximum efficiency (assuming $P_{TF} = P_T$). It can be seen from Eq. (A-2) (and has been pointed out by Silver) that uniform illumination is obtained if

$$\begin{aligned} G_f(\psi, \xi) &= \sec^4(\psi/2) \qquad 0 < \psi < \Psi \\ G_f(\psi, \xi) &= 0 \qquad\qquad\quad \Psi < \psi < \pi \end{aligned} \tag{28}$$

From a comparison of Eq. (27) and (28) it can be seen that uniform aperture illumination will be present if

$$G_H(\gamma, \xi_H) \approx M^2 \tag{29}$$

In the case of a 90-deg aperture angle ($f/D = 0.25$), for example, uniform hyperboloid illumination results in uniform paraboloid aperture illumination. To achieve the same result from the focal point, a 6-db reverse taper would be required. It should be noted, however, that in principle a focal-plane feed could be built which would have the same source current distribution as the hyperboloid in a Cassegrainian system.

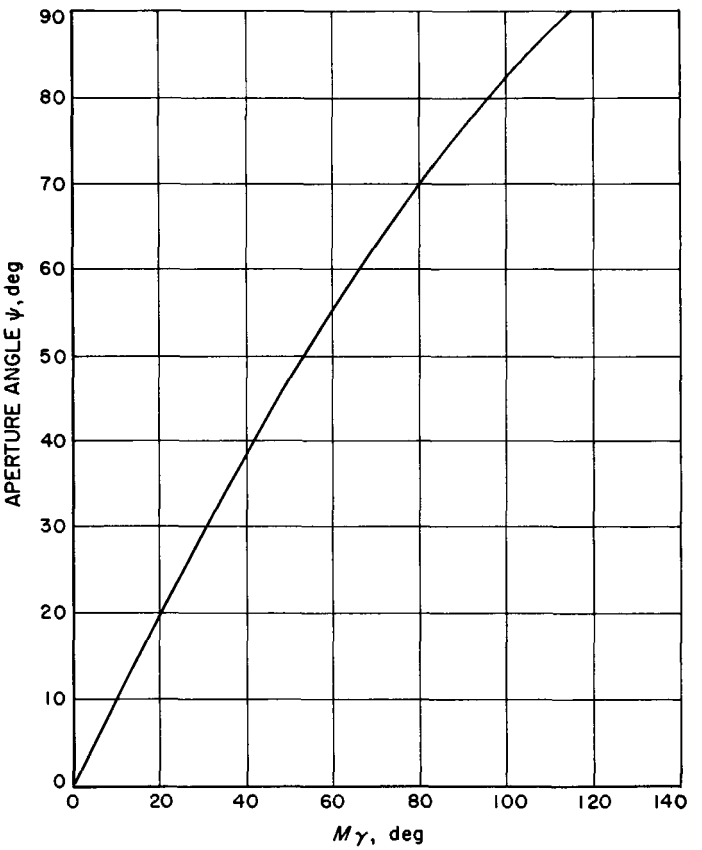


**Figure 8. Relationship between $M\gamma$ and $\psi$**

# IV. ANALYSIS OF ERRORS

Several possible sources of error are analyzed in this Section. The following errors are considered: polarization loss, aperture phase deviations, azimuthal sampling error, and aperture blockage.

In general, it is not practical to assign an exact value to the errors, but only to indicate their approximate values. However, since sound design will reduce these errors to a small value, a relatively inaccurate determination of the errors can nonetheless result in highly accurate determination of the over-all efficiency.

## A. Polarization Loss

It has been pointed out by Silver and also by Cutler (Ref. 7) that a cross-polarized component will exist in the aperture which does not contribute to the axial secondary radiation and which therefore introduces a loss of efficiency. This efficiency loss is a function of the feed radiation properties. In Appendix B this loss is analyzed for the case of a small dipole feed, parallel to the axis $X$ at the second focus of a Cassegrainian system. In this case the aperture field components are given by

$$\frac{E_X}{E_0} = 1 - \cos^2\xi\,(1-\cos\gamma) \qquad \textit{Cassegrainian Feed} \qquad (30)$$

$$\frac{E_Y}{E_0} = \tfrac{1}{2}\sin 2\xi\,(1-\cos\gamma) \qquad (31)$$

For the case of a dipole feed at the focal point, the angle $\gamma$ is replaced by the aperture angle $\psi$:

$$\frac{E_X}{E_0} = 1 - \cos^2\xi\,(1-\cos\psi) \qquad \textit{Focal-Point Feed} \qquad (32)$$

$$\frac{E_Y}{E_0} = -\tfrac{1}{2}\sin 2\xi\,(1-\cos\psi) \qquad (33)$$

A question of semantics arises in the interpretation of Eq. (30) through (33). In the derivation of these relationships a specific type of feed radiation function—that of a small dipole—is assumed. It is sometimes erroneously concluded that Eq. (32) and (33) inevitably dictate low efficiency for a deep paraboloid. That this is not true can be easily seen by comparison of Eq. (30) and (31) with (32) and (33). In the former case, the polarization loss is small, since the angle $\gamma$ is small. Furthermore, it is theoretically possible to design a focal-point feed with the same radiation pattern (and hence polarization loss) as the hyperboloid in a Cassegrainian feed system. Thus, it does not appear appropriate to combine directly Eq. (32) and Eq. (1) to determine polarization loss. Rather, a more direct measure of the polarization loss is achieved by comparing the efficiency obtained by integration of Eq. (32) across the aperture to that obtained by integration of the total field across the aperture. Thus, from Eq. (A-11) the polarization loss factor $\eta_p$ is given by

$$\eta_p \equiv \frac{\left|\int_0^{2\pi}\int_0^{\Psi}\frac{E_X}{E_0}(\psi,\xi)\tan\left(\frac{\psi}{2}\right)d\psi\,d\xi\right|^2}{\left|\int_0^{2\pi}\int_0^{\Psi}\sqrt{\left(\frac{E_X}{E_0}\right)^2+\left(\frac{E_Y}{E_0}\right)^2}\tan\left(\frac{\psi}{2}\right)d\psi\,d\xi\right|^2} \qquad (34)$$

By appropriate choice of the $f/D$ ratio and/or the feed system, the following is generally true:

$$\frac{E_Y}{E_0} << \frac{E_X}{E_0} \qquad (35)$$

In this case,

$$\sqrt{\left(\frac{E_X}{E_0}\right)^2+\left(\frac{E_Y}{E_0}\right)^2} \approx \frac{E_X}{E_0}\left(1+\tfrac{1}{2}\frac{E_Y^2}{E_X^2}\right) = \frac{E_X}{E_0}+\tfrac{1}{2}\frac{E_Y}{E_X}\frac{E_Y}{E_0} \qquad (36)$$

It is convenient to define two quantities, $I_1$ and $I_2$, as follows:

$$I_1 \equiv \int_0^{2\pi}\int_0^{\Psi}\frac{E_X}{E_0}(\psi,\xi)\tan\left(\frac{\psi}{2}\right)d\psi\,d\xi \qquad (37)$$

$$I_2 \equiv \int_0^{2\pi}\int_0^{\Psi}\frac{E_Y}{E_X}\frac{E_Y}{E_0}(\psi,\xi)\tan\left(\frac{\psi}{2}\right)d\psi\,d\xi \qquad (38)$$

Combining Eq. (34), (36), (37), and (38) yields

$$\eta_p \approx \frac{|I_1|^2}{|I_1+\tfrac{1}{2}I_2|^2} \qquad (39)$$

Since both $I_1$ and $I_2$ are positive real quantities and $I_2 << I_1$, we have

$$\eta_p \approx \frac{I_1^2}{(I_1-\tfrac{1}{2}I_2)^2} = \frac{I_1^2}{I_1^2+I_1I_2} = \frac{1}{1+\frac{I_2}{I_1}} \qquad (40)$$

$$\eta_p \approx 1 - \frac{I_2}{I_1} \qquad (41)$$

Also, from Eq. (32), (33), (37), and (38),

$$\frac{I_2}{I_1} \approx \frac{\tfrac{1}{4}\int_0^{2\pi}\int_0^{\Psi}\sin^2 2\xi\,(1-\cos\psi)^2\tan\left(\frac{\psi}{2}\right)d\psi\,d\xi}{\int_0^{2\pi}\int_0^{\Psi}\tan\left(\frac{\psi}{2}\right)d\psi\,d\xi} \qquad (42)$$

$$= \tfrac{1}{8}\frac{\int_0^{\Psi}(1-\cos\psi)^2\tan\left(\frac{\psi}{2}\right)d\psi}{\int_0^{\Psi}\tan\left(\frac{\psi}{2}\right)d\psi} \qquad (43)$$

In order to express Eq. (43) in a simpler form, it is convenient to use the approximation

$$\cos\psi \approx 1 - \frac{\psi^2}{2} \tag{44}$$

This approximation is in error by only 5% for values of $\psi$ as large as 60 deg. Combining Eq. (43) and (44),

$$\frac{I_2}{I_1} \approx \frac{1}{32} \frac{\int_0^{\Psi} \psi^4 \tan\left(\frac{\psi}{2}\right) d\psi}{\int_0^{\Psi} \tan\left(\frac{\psi}{2}\right) d\psi} \tag{45}$$

An additional approximation will now be made:

$$\tan\frac{\psi}{2} \approx \frac{\psi}{2} \tag{46}$$

This approximation is in error by 8% at 60 deg, unfortunately in the same direction (downward) as that of Eq. (44). Combining Eq. (45) and (46),

$$\frac{I_2}{I_1} \approx \frac{1}{32} \frac{\int_0^{\Psi} \psi^5 \, d\psi}{\int_0^{\Psi} \psi \, d\psi} \tag{47}$$

Performing the integration gives

$$\frac{I_2}{I_1} \approx \frac{1}{96} \Psi^4 \tag{48}$$

where $\Psi$ is measured in radians. Combining Eq. (41) and (48) yields the approximate polarization loss for a focal-point, dipole-like feed:

$$\boxed{\eta_p \approx 1 - \frac{1}{96}\Psi^4} \qquad \Psi < 1 \tag{49}$$

It is clear from Eq. (48) that the approximation used in Eq. (40) and (41) is very good.

The approximate polarization loss in a Cassegrainian feed system is easily derived. For this case Eq. (45) has to be modified:

$$\frac{I_2}{I_1} \approx \frac{1}{32} \frac{\int_0^{\Psi} \gamma^4 \tan\left(\frac{\psi}{2}\right) d\psi}{\int_0^{\Psi} \tan\left(\frac{\psi}{2}\right) d\psi} \tag{50}$$

From Eq. (10) it can be seen that

$$\gamma \approx \frac{2}{M} \tan\left(\frac{\psi}{2}\right) \tag{51}$$

Combining Eq. (50) and (51),

$$\frac{I_2}{I_1} \approx \frac{1}{2M^4} \frac{\int_0^{\Psi} \tan^5\left(\frac{\psi}{2}\right) d\psi}{\int_0^{\Psi} \tan\left(\frac{\psi}{2}\right) d\psi} \tag{52}$$

$$\frac{I_2}{I_1} = \frac{\frac{1}{4}\tan^4\left(\frac{\Psi}{2}\right) - \left[\frac{1}{2}\tan^2\left(\frac{\Psi}{2}\right) + \ln\cos\left(\frac{\Psi}{2}\right)\right]}{2M^4 \left|\ln\sec\left(\frac{\Psi}{2}\right)\right|} \tag{53}$$

From Eq. (41) we have

$$\eta_p \approx 1 - \frac{1}{2M^4} \frac{\frac{1}{4}\tan^4\left(\frac{\Psi}{2}\right) - \left[\frac{1}{2}\tan^2\left(\frac{\Psi}{2}\right) + \ln\cos\left(\frac{\Psi}{2}\right)\right]}{\ln\left|\sec\left(\frac{\Psi}{2}\right)\right|} \tag{54}$$

The polarization loss for various values of $M$ is shown in Fig. 9. It can be seen that the polarization loss is exceedingly small for $M > 2$ (usually $2 < M < 10$), even for very deep paraboloids. There is some experimental verification of this fact: Foldes (Ref. 3) has reported high over-all aperture efficiencies for the case of $\Psi = 104$ deg. The case of $M = 1$ corresponds to a focal-point feed and was plotted from Eq. (49). It can be seen here that the polarization loss rapidly becomes serious as a 60-deg aperture angle is approached.

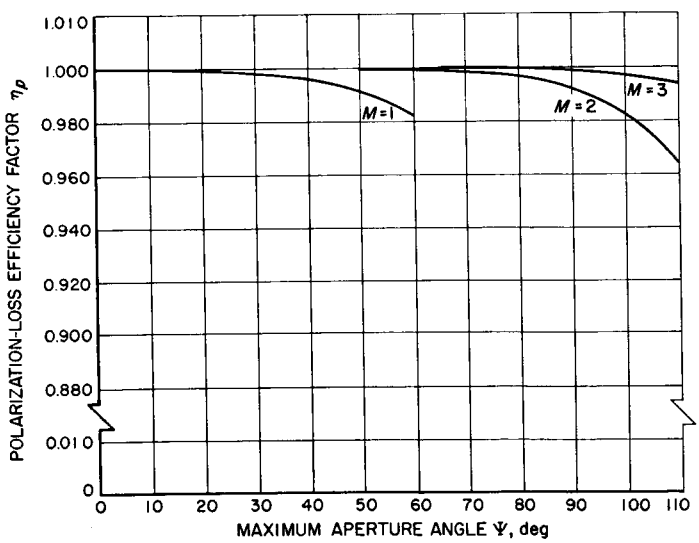


**Figure 9. Cross-polarization loss**

It should be pointed out that normal measurement of the linear polarized feed patterns $G_{fn}(\psi, \xi_n)$ automatically takes the polarization loss into account. If the feed and illuminator polarization are aligned on axis ($\psi = 0$), then

at other values of $\psi$ the illuminator will respond only to the desired feed polarization component. The measured gain of the feed $G_{0f}$ will, on the other hand, be determined by power radiated in all polarization components.

### B. Aperture Phase Errors

In the derivation of Eq. (1), it is assumed that the phase front from the paraboloid focus is truly spherical—i.e., that there are no phase deviations—and furthermore that the paraboloid has no surface deformities. This happy situation is never completely realized in practice. In general, both surface deviations and feed phase-front errors will exist.

The problem of normally distributed aperture phase errors has been treated by Ruze (Ref. 8) and also by Robieux (Ref. 9). Their analyses are specifically directed toward tolerance errors in the paraboloid, but are equally applicable to the feed phase-front errors. Unfortunately, a shallow paraboloid is assumed, which makes their results somewhat pessimistic for the case of a low $f/D$ antenna. For a small rms phase error of $\delta$ radians, Ruze derives the approximate tolerance efficiency factor $\eta_T$:

$$\eta_T \approx \varepsilon^{-\delta^2} \tag{55}$$

In Fig. 10 the factor $\eta_T$ is shown as a function of the paraboloid aperture error in degrees. This Figure is a plot of Eq. (55) and, hence, assumes a shallow reflector, uniform illumination, and a normal error distribution.

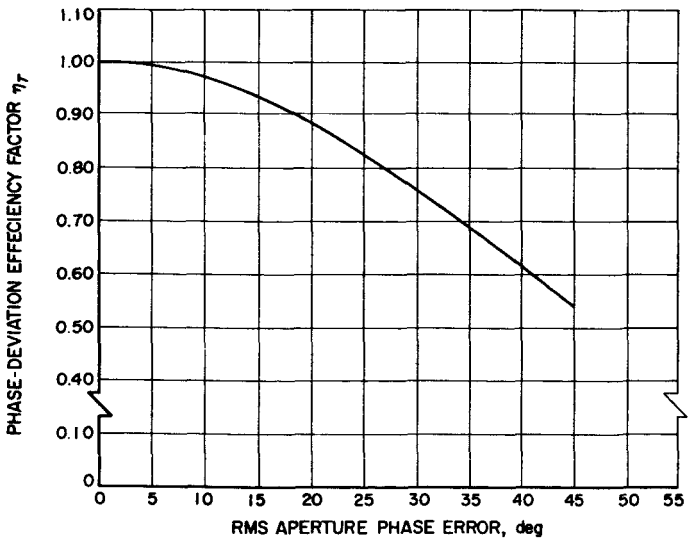


**Figure 10. Efficiency loss due to random aperture phase errors**

The serrodyne system (Ref. 10) may be conveniently used to measure the feed-system phase characteristics. The block diagram of a typical setup for phase-front measurements is shown in Fig. 11. Typically the results of such measurements indicate two separate components of error, a more-or-less quadratic deviation, and a high-frequency semiperiodic error. The former source of error has been treated by Silver and others and, in practice, can be largely corrected by feed defocusing. The high-frequency component is virtually inevitable in the case of Cassegrainian or shaped-beam feeds in which phase ripples occur at an angular frequency corresponding to the hyperboloid (or shaped-beam feed) size in wavelengths. The distribution across the aperture may be more nearly sinusoidal than normal. The use of Eq. (55) will, in this case, yield a somewhat pessimistic result since large phase excursions above the rms level are less probable for a sinusoidal distribution than for a normal distribution. Equation (55) may be reasonably used for small deviations, however, without introducing undue error in the over-all efficiency.

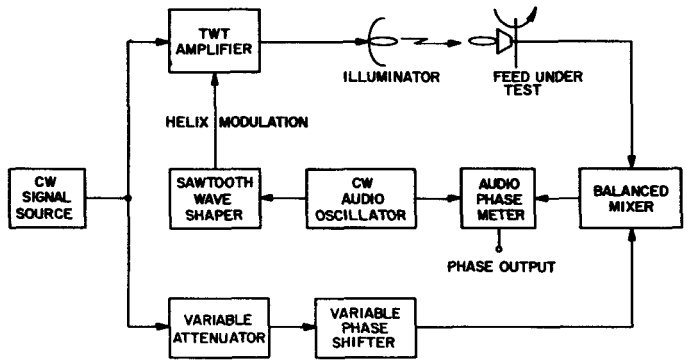


**Figure 11. Serrodyne system for the measurement of the feed phase front**

### C. Azimuthal Sampling Errors

In using Eq. (1) to determine aperture efficiency, one is approximating the azimuthal or $\xi$ dependence by a discrete sampling process. This procedure is used for pattern measurement convenience. An error is, of course, introduced by this procedure; but the approximate magnitude of the error may be estimated.

It is convenient in the error analysis to assume that the feed radiation function is separable into two functions which are functions only of either $\psi$ or $\xi$. With this assumption, Eq. (1) becomes

$$\eta = \cot^2\left(\frac{\Psi}{2}\right) G_{0f} \left| \left[ \int_0^{\Psi} E_{f\psi}(\psi) \tan\left(\frac{\psi}{2}\right) d\psi \right] \times \left[ \frac{1}{N} \sum^{N} E_{f\xi}(\xi_N) \right] \right|^2 \tag{56}$$

The sampling error $\eta_S$ is thus given by

$$\eta_S = \frac{\left[\frac{1}{N}\sum^{N} E_f \xi_n (\xi_n)\right]^2}{\left[\frac{1}{2\pi}\int_0^{2\pi} E_{f\xi}(\xi)\, d\xi\right]^2} \tag{57}$$

or

$$\eta_S = \frac{\left[\frac{1}{2\pi}\sum^{N} E_f\, \xi_n (\xi_n)\frac{2\pi}{N}\right]^2}{\left[\frac{1}{2\pi}\int_0^{2\pi} E_{f\xi}(\xi)\, d\xi\right]^2} = \frac{[\sum^{N} E_f \xi_n (\xi_n)\,\Delta\xi]^2}{\left[\int_0^{2\pi} E_{f\xi}(\xi)\, d\xi\right]^2} \tag{58}$$

where $\Delta\xi = 2\pi/N$. It is possible to expand the function $E_{f\xi}(\xi)$ in a Taylor series about the point $\xi = \xi_n$:

$$E_{f\xi}(\xi) = \frac{E_{f\xi}(\xi_n)}{0!} + \frac{(\xi - \xi_n) E'_{f\xi}(\xi_n)}{1!} + \frac{(\xi - \xi_n)^2 E''_{f\xi}(\xi_n)}{2!} + \cdots \tag{59}$$

Integrating both sides of Eq. (59) between the points $\xi_n + (\Delta\xi/2)$ and $\xi_n - (\Delta\xi/2)$ results in

$$\int_{\xi_n-(\Delta\xi/2)}^{\xi_n+(\Delta\xi/2)} E_{f\xi}(\xi)\, d\xi = E_{f\xi}(\xi_n)\,\Delta\xi + 0 + \frac{1}{24} E''_{f\xi}(\xi_n)(\Delta\xi)^3 + \cdots \text{ odd-order terms} \tag{60}$$

Neglecting higher-order terms,

$$E_{f\xi}(\xi_n)\,\Delta\xi \approx \left[\int_{\xi_n-(\Delta\xi/2)}^{\xi_n+(\Delta\xi/2)} E_{f\xi}(\xi)\, d\xi\right] - \frac{1}{24} E''_{f\xi}(\xi_n)(\Delta\xi)^3 \tag{61}$$

or

$$\sum^{N} E_{f\xi}(\xi_n)\,\Delta\xi \approx \left[\int_0^{2\pi} E_{f\xi}(\xi)\, d\xi\right] - \frac{1}{24}\sum^{N} E''_{f\xi}(\xi_n)\left(\frac{2\pi}{N}\right)^3 \tag{62}$$

Combining Eq. (58) and (62),

$$\eta_S \approx \left[1 - \frac{1}{24}\frac{\sum^{N} E''_{f\xi}(\xi_n)\left(\frac{2\pi}{N}\right)^3}{\int_0^{2\pi} E_{f\xi}(\xi)\, d\xi}\right]^2 \tag{63}$$

Now, making the approximation that the integral in Eq. (63) is given by the numerator in Eq. (58),

$$\eta_S \approx \left[1 - \frac{1}{24}\frac{\sum^{N} E''_{f\xi}(\xi_n)\left(\frac{2\pi}{N}\right)^3}{\sum^{N} E_{f\xi}(\xi_n)\frac{2\pi}{N}}\right]^2 \tag{64}$$

or

$$\eta_S \approx \left[1 - \frac{1.65}{N^2}\frac{\frac{1}{N}\sum^{N} E''_{f\xi}(\xi_n)}{\frac{1}{N}\sum^{N} E_{f\xi}(\xi)}\right]^2 \tag{65}$$

It can be seen from Eq. (65) that the error is controlled basically by the ratio of the average value of the second derivative of the azimuthal function to the average value of the function. Furthermore, the error is rapidly decreased by increasing the number of cuts, or samples.

### D. Aperture Blockage

It generally happens that obscuration of the paraboloid aperture will result from the presence of the feed system and its support structure. This problem may be conveniently divided into two cases: in the first, the obstacle is interposed between the focal point and the surface of the paraboloid; in the second, the obstacle is between the surface of the paraboloid and a plane perpendicular to the axis and in front of the antenna. In unusual circumstances an obstacle may be in both categories, although sound design will generally avoid this situation.

Blocking of the first type may be legitimately considered part of feed-system radiation characteristics. As such it may be either evaluated by geometrical optics or (preferably) included physically in the feed-system pattern-determination model.

Blockage of the second type may be conveniently evaluated only if the cross sections of the obstacle are moderately large in terms of a wavelength. In this case, it is reasonable to assume that a well-defined shadow region will occur on the aperture. The procedure then is to determine the shadow region on the aperture and to assign zero intensity to the corresponding part of $G_{f\xi}(\psi, \xi)$. Since over-all blockage areas typically correspond to only 1–5% of the antenna aperture, the accuracy of the antenna efficiency is not unduly sensitive to the accuracy of the blockage calculation.

# V. CONCLUSION

A simple graphical technique has been developed for the determination of paraboloidal antenna efficiency as a function of the feed-system radiation characteristics. The technique has been applied in detail to the Cassegrainian feed system. In this system, the transformation of the feed radiation pattern into the aperture illumination function has been analyzed and shown to possess certain desirable properties from the standpoint of efficiency.

A short analysis has been made of various errors involved in the efficiency calculation. The effect of cross-polarized field components in the aperture is shown to be small for Cassegrainian systems or their shaped-beam feed equivalents. The effect of discrete sampling of non-symmetrical feed patterns has been analyzed and the corresponding errors evaluated. Finally, methods for determining the effect of aperture phase errors and obstacle blockage have been discussed.

## Acknowledgement

The author gratefully acknowledges many stimulating discussions on Cassegrainian systems with Peter Foldes of RCA Victor, Montreal.

The use of the serrodyne technique for measurement of feed-pattern phase characteristics was suggested by Paul Cramer of the Jet Propulsion Laboratory, and later extended and developed by Danver Schuster of JPL. Finally, the author wishes to thank William Merrick of JPL, whose many penetrating questions created the motivation for this report.

# NOMENCLATURE

| | |
|---|---|
| $a, c$ | constants describing the hyperboloid |
| $\mathbf{a}_X, \mathbf{a}_Y, \mathbf{a}_\gamma, \mathbf{a}_\xi, \mathbf{a}_\psi, \mathbf{a}_{\xi_H}$ | unit vectors in the $X$, $Y$, $\gamma$, $\xi$, $\psi$, and $\xi_H$ directions |
| $\Delta A$ | an incremental area |
| $D$ | diameter of the paraboloid |
| $e_{ix}$ | $X$ component of the paraboloid aperture field |
| $E'_{f\xi}, E''_{f\xi}(\xi_n)$ | first and second derivatives with respect to $\xi$ |
| $E_0$ | dipole field strength for polarization analysis |
| $E_{f\xi}(\xi)$ | feed pattern for a particular value of $\psi$ |
| $E_{fn}(\psi, \xi_n)$ | field-strength feed pattern for a particular azimuthal coordinate |
| $E_X, E_Y$ | $X$ and $Y$ components of $E_0$ |
| $\mathbf{E}_X, \mathbf{E}_Y, \mathbf{E}_r, \mathbf{E}_\gamma, \mathbf{E}_{\xi_H}, \mathbf{E}_\psi, \mathbf{E}_\xi$ | dipole field-strength components in the $X$, $Y$, $r$, $\gamma$, $\xi_H$, $\psi$, and $\xi$ directions |
| $\mathbf{E}(F')$ | vector dipole field strength |
| $\mathbf{E}(R_0, 0, 0)$ | antenna-system axial-vector far-field strength |
| $E(R_0, 0, 0)$ | antenna-system far-field strength |
| $E^*(R_0, 0, 0)$ | complex conjugate of $E(R_0, 0, 0)$ |
| $f$ | focal length of the paraboloid |
| $F$ | focal point of the paraboloid |
| $F'$ | second focal point of the hyperboloid |
| $G$ | gain of the antenna system |
| $G_f(\psi, \xi)$, $G'_f(\psi, \xi)$ | gain functions for the subreflector |
| $G_H(\gamma, \xi_H)$ | gain function for the feedhorn |
| $G_{0f}$ | maximum power gain of a focal-point feed system |
| $h$ | ordinate of the aperture integration plot |
| $I_{n0}(\Psi)$ | aperture integral for uniform illumination |
| $I_1, I_2$ | integrals for polarization analysis |
| $j$ | $\sqrt{-1}$ |
| $k$ | propagation constant |
| $\Delta l, \Delta l_r$ | incremental distance on the hyperboloid |
| $M$ | magnification factor |
| $\mathbf{n}$ | vector normal to the reflector surface |
| $N$ | number of feed-pattern azimuthal samples |
| $P$ | arbitrary point on reflector surface |
| $P(\psi, \xi)$ | power flux from the subreflector |
| $P(0, 0)$ | antenna-system axial far-field strength |
| $P_H(\gamma, \xi_H)$ | power flux from the feedhorn |

## NOMENCLATURE (Cont'd)

| | |
|---|---|
| $P_T$ | total power radiated by the feedhorn |
| $P_{TF}$ | total power radiated by the subreflector |
| $r$ | radial coordinate from the antenna axis |
| $r, \gamma, \xi_H$ | polar coordinates of the hyperboloid |
| $r_1, r_2$ | magnitudes of $\mathbf{r}_1$ and $\mathbf{r}_2$ |
| $\mathbf{r}_1, \mathbf{r}_2$ | vector distances from the hyperboloid to its foci |
| $R, \theta, \phi$ | polar coordinates of the far field |
| $R_0$ | distance to point in the far field |
| $w, w'(\psi)$ | abscissas of the aperture integration plot |
| $\Delta w$ | incremental width on the aperture |
| $X, Y, Z$ | rectangular coordinates of the paraboloid |
| $X_H, Y_H, Z_H$ | rectangular coordinates of the hyperboloid |
| $\gamma_0$ | maximum half-angle subtended by the hyperboloid |
| $\Delta\gamma, \Delta\xi_H, \Delta\psi, \Delta\xi$ | incremental changes of the coordinates |
| $\delta$ | aperture phase error |
| $\varepsilon$ | permittivity |
| $\eta$ | over-all aperture efficiency |
| $\eta_p$ | polarization-loss efficiency factor |
| $\eta_S$ | sampling-error efficiency factor |
| $\eta_T$ | phase-deviation efficiency factor |
| $\lambda$ | wavelength |
| $\mu$ | permeability |
| $\xi_n$ | azimuthal coordinate of a particular feed pattern |
| $\rho, \psi, \xi$ | polar coordinates of the paraboloid |
| $\rho$ | distance from the paraboloid surface to its focus |
| $\Psi$ | maximum aperture half-angle of the paraboloid |
| $\omega$ | angular frequency |
| $\Delta\Omega_H, \Delta\Omega$ | incremental solid angles |

## REFERENCES


1. Silver, S., *Microwave Antenna Theory and Design,* McGraw-Hill, New York, 1949.
2. Doundoulakis, G., and Gethin, S., *Far Field Patterns of Circular Paraboloidal Reflectors,* IRE National Convention Record, Part I, 1959.
3. Foldes, P., and Komlos, S., "Theoretical and Experimental Study of Wide Band Paraboloid Antennas with Central Reflector Feed," *RCA Review,* vol. XXI (1):94–116, March, 1960.
4. Foldes, P., *Ground Antenna Parameters Affecting the Range of a Space Communications System,* Report No. 3457-F, RCA Victor Co., Ltd., Montreal, Canada.
5. Hannon, P. W., "Microwave Antennas Derived from the Cassegrain Telescope," *IRE Transactions on Antennas and Propagation,* vol. AP-9 (2):140–153, March, 1961.
6. Salomonovich, A. F., and Soboleva, N. S., "Design of a Two-Mirror Radiotelescope," *Radiotekhnika i elektronika, 4 (5):799–804, 1959.*
7. Cutler, C. C., "Parabolic-Antenna Design for Microwaves," *Proceedings of the IRE,* pp. 1284–1294, November, 1947.
8. Ruze, J., *Effect of Aperture Distribution Errors on the Radiation Pattern,* Antenna Lab Memo, Air Force Cambridge Research Center, January 22, 1952.
9. Robieux, J., "Influence of the Manufacturing Accuracy of an Antenna on its Performance," *Annales de Radioelectricité,* January, 1956.
10. Cumming, R. C., "The Serrodyne Frequency Translator," *Proceedings of the IRE,* vol. 45:175–186, February, 1957.

# APPENDIX A

## Derivation of the Aperture Integral

The method used here to calculate the aperture integral is that used by Silver (Ref. 1, Chap. 12), modified to permit variation in the $\xi$ coordinate, which is generally observed in practice. The paraboloid geometry is depicted in Fig. 1. By expressing the current density on the surface of the paraboloid as a function of the feed gain function $G_f(\psi, \xi)$, and projecting this current density onto the aperture plane of the paraboloid, Silver derives an expression for the axial field intensity $E(R_0, 0, 0)$:

$$\mathrm{E}(R_0, 0, 0) = \mathrm{a}_X \frac{j\omega\mu}{2\pi R_0} e^{-jkR_0} \left[\left(\frac{\varepsilon}{\mu}\right)^{1/2} \frac{P_T}{2\pi}\right]^{1/2} \times \int_0^{2\pi} \int_0^{\Psi} e_{ix} [G_f(\psi, \xi)]^{1/2} e^{-jk\rho} (1 + \cos^4) \rho \sin\psi \, d\psi \, d\xi \tag{A-1}$$

In this case, linear polarization is assumed. Normally, the factor $e_{ix}$, which is the $X$ component of the aperture plane polarization, is assumed constant and equal to unity. For paraboloids whose aperture angle $\Psi$ approaches 90 deg, this approximation is poor. The problem can be circumvented, however, by measuring the pattern $G_f(\psi)$ as outlined in Sec. IV. For this reason, $e_{ix}$ will be eliminated from further consideration.

The equation of the paraboloid is given by

$$\rho = \frac{2f}{1 + \cos\psi} = f \sec^2\left(\frac{\psi}{2}\right) \tag{A-2}$$

Combining Eq. (A-1) and (A-2) gives

$$\mathrm{E}(R_0, 0, 0) = \mathrm{a}_X \frac{ja\mu f}{\pi R_0} e^{-jk(R_0 + 2f)} \left[\left(\frac{\varepsilon}{\mu}\right)^{1/2} \frac{P_T}{2\pi}\right]^{1/2} \int_0^{2\pi} \int_0^{\Psi} [G_f(\psi, \xi)]^{1/2} \tan\left(\frac{\psi}{2}\right) d\psi \, d\xi \tag{A-3}$$

The squared magnitude of the electric field is given by

$$|E(R_0, 0, 0)|^2 = E(R_0, 0, 0) E^*(R_0, 0, 0) = \frac{\omega^2\mu^2 f^2}{\pi^2 R_0^2} \left(\frac{\varepsilon}{\mu}\right)^{1/2} \frac{P_T}{2\pi} \left| \int_0^{2\pi} \int_0^{\Psi} [G_f(\psi, \xi)]^{1/2} \tan\left(\frac{\psi}{2}\right) d\psi \, d\xi \right|^2 \tag{A-4}$$

The power per unit solid angle $P(0, 0)$ radiated in the forward direction is given by

$$P(0, 0) = \tfrac{1}{2} R_0^2 \left(\frac{\varepsilon}{\mu}\right)^{1/2} |E(R_0, 0, 0)|^2 \tag{A-5}$$

Combining Eq. (A-4) and (A-5) and substituting $4\pi^2/\lambda^2$ for $\omega^2\mu^\varepsilon$,

$$P(0, 0) = \frac{P_T}{\pi\lambda^2} f^2 \left| \int_0^{2\pi} \int_0^{\Psi} [G_f(\psi, \xi)]^{1/2} \tan\left(\frac{\psi}{2}\right) d\psi \, d\xi \right|^2 \tag{A-6}$$

The antenna gain is given by

$$G = \frac{P(0, 0)}{\frac{P_T}{4\pi}} \tag{A-7}$$

Combining Eq. (A-6) and (A-7) yields

$$G = \frac{4f^2}{\lambda^2}\left|\int_0^{2\pi}\int_0^{\Psi}[G_f(\psi,\xi)]^{1/2}\tan\left(\frac{\psi}{2}\right)d\psi\,d\xi\right|^2 \tag{A-8}$$

Now the following paraboloid relationship is introduced:

$$f = \frac{D}{4}\cot\frac{\Psi}{2} \tag{A-9}$$

Combining Eq. (A-8) and (A-9) gives

$$G = \tfrac{1}{4}\left(\frac{D}{\lambda}\right)^2\cot^2\left(\frac{\Psi}{2}\right)\left|\int_0^{2\pi}\int_0^{\Psi}[G_f(\psi,\xi)]^{1/2}\tan\left(\frac{\psi}{2}\right)d\psi\,d\xi\right|^2 \tag{A-10}$$

Introducing the concepts of the relative voltage pattern, $E_f(\psi,\xi)$, and the feed gain, $G_{0f}$,

$$G = \tfrac{1}{4}\left(\frac{D}{\lambda}\right)^2\cot^2\left(\frac{\Psi}{2}\right)G_{0f}\left|\int_0^{2\pi}\int_0^{\Psi}E_f(\psi,\xi)\tan\left(\frac{\psi}{2}\right)d\psi\,d\xi\right|^2 \tag{A-11}$$

The aperture is now divided into $N$ equal segments such that $E_f(\psi,\xi)$ is essentially constant over the segment in the $\xi$ direction and equal to $E_{fn}(\psi,\xi_n)$. Thus,

$$G = \tfrac{1}{4}\left(\frac{D}{\lambda}\right)^2\cot^2\left(\frac{\Psi}{2}\right)G_{0f}\left|\frac{2\pi}{N}\sum_{n=1}^{n=N}\int_0^{\Psi}E_{fn}(\psi,\xi_n)\tan\left(\frac{\psi}{2}\right)d\psi\right|^2 \tag{A-12}$$

or

$$G = \eta\left(\frac{\pi D}{\lambda}\right)^2 \tag{A-13}$$

where the antenna efficiency $\eta$ is given by

$$\boxed{\eta = \cot^2\left(\frac{\Psi}{2}\right)G_{0f}\left|\frac{1}{N}\sum_{n=1}^{n=N}\int_0^{\Psi}E_{fn}(\psi,\xi_n)\tan\left(\frac{\psi}{2}\right)d\psi\right|^2} \tag{A-14}$$

Equation (A-14) is termed the aperture illumination integral. The choice of the number $N$ and the other approximation errors are discussed in Sec. IV.

# APPENDIX B

## Polarization Transformation of the Cassegrainian Feed System

The coordinate system used for the polarization transformation analysis is shown in Fig. B-1. The field at the point $F$ is assumed to be given by

$$\mathbf{E}(F') = E_0 \mathbf{a}_X \tag{B-1}$$

The projection of this vector onto the line defined by the intersection of the $Z = 0$ plane and the $\xi =$ constant plane is given by

$$\mathbf{E}_\gamma(\xi_H, \gamma = 0) = E_0 \cos \xi_H \mathbf{a}_\gamma \tag{B-2}$$

The projection of this vector onto a plane normal to the line $FP$ is given by

$$\mathbf{E}_\gamma(\xi_H, \gamma) = E_0 \cos \xi_H \cos \gamma \mathbf{a}_\gamma \tag{B-3}$$

Similarly it can be seen that

$$\mathbf{E}_{\xi_H}(\xi_H, \gamma) = E_0 \sin \xi_H \mathbf{a}_{\xi_H} \tag{B-4}$$

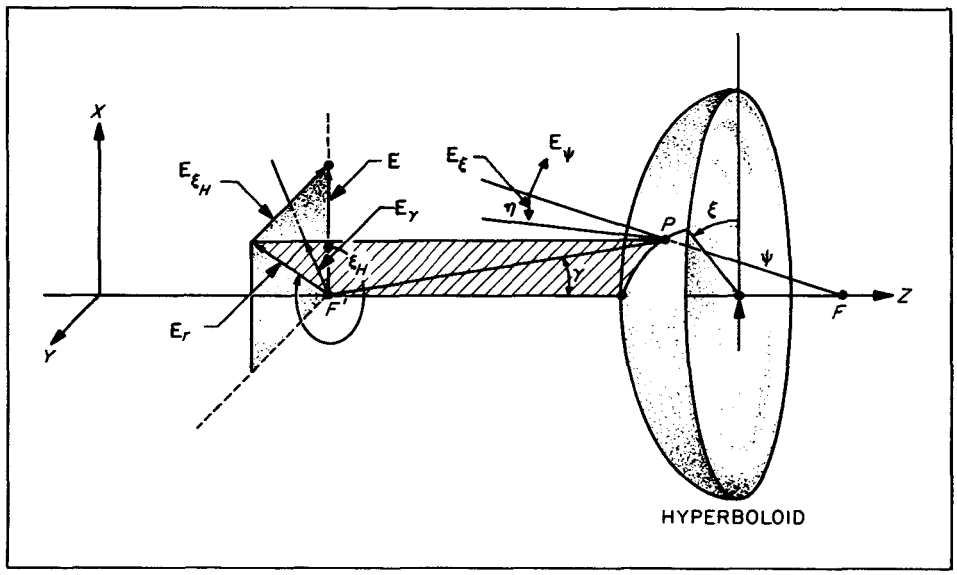


**Figure B-1. Polarization analysis geometry**

It was shown in Eq. (18) through (20) that the relative intensities of the $\xi$ and $\psi$ components of the field are preserved in reflection from the hyperboloid. This can also be easily seen from consideration of the normal and tangential field components at the hyperboloid surface. Thus,

$$\mathbf{E}_\psi = -E_0 \cos \xi \cos \gamma \mathbf{a}_\psi \tag{B-5}$$

$$\mathbf{E}_\xi = -E_0 \sin \xi - \mathbf{a}_\xi = E_0 \sin \xi \mathbf{a}_\xi \tag{B-6}$$

The minus signs in Eq. (B-5) and (B-6) arise from the change of coordinates and the zero tangential field restriction.

Since the paraboloid will transform rays from the point $F$ into rays normal to the $X$–$Y$ plane, the polarization in the aperture plane will be given by the $X$ and $Y$ components of Eq. (B-5) and (B-6). From Fig. B-1 it can be seen that

$$\mathbf{E}_X = (\mathbf{E}_\psi \cdot \mathbf{a}_\psi \cos\xi - \mathbf{E}_\xi \cdot \mathbf{a}_\xi \sin\xi)\,\mathbf{a}_X \tag{B-7}$$

$$\mathbf{E}_\psi = (\mathbf{E}_\psi \cdot \mathbf{a}_\psi \sin\xi + \mathbf{E}_\xi \cdot \mathbf{a}_\xi \cos\xi)\,\mathbf{a}_\psi \tag{B-8}$$

Combining Eq. (B-5), (B-6), (B-7), and (B-8) gives

$$\frac{\mathbf{E}_X}{E_0} = (-\cos^2\xi\cos\gamma - \sin^2\xi)\,\mathbf{a}_X$$

$$\boxed{\frac{\mathbf{E}_X}{E_0} = -\left[1 - \cos^2\xi\,(1 - \cos\gamma)\right]\mathbf{a}_X} \tag{B-9}$$

and

$$\frac{\mathbf{E}_Y}{E_0} = (-\sin\xi\cos\xi\cos\gamma + \sin\xi\cos\xi)\,\mathbf{a}_Y$$

$$\boxed{\frac{\mathbf{E}_Y}{E_0} = \tfrac{1}{2}\sin 2\xi\,(1 - \cos\gamma)\,\mathbf{a}_Y} \tag{B-10}$$

It should be noted that Eq. (B-9) and (B-10) are not functions of the aperture angle $\psi$, except insofar as $\gamma$ and $\psi$ are related in Eq. (10).